2024 IEEE/RSJ International Conference on Intelligent Robots and Systems (IROS)
October 14-18, 2024. Abu Dhabi, UAE

A Unified Interaction Control Framework for Safe Robotic Ultrasound Scanning with Human-Intention-Aware Compliance

Xiangjie Yan, Shaqi Luo, Yongpeng Jiang, Mingrui Yu, Chen Chen,
Senqiang Zhu, Gao Huang, Shiji Song and Xiang Li

***Abstract*— The ultrasound scanning robot operates in environments where frequent human-robot interactions occur. Most existing control methods for ultrasound scanning address only one specific interaction situation or implement hard switches between controllers for different situations, which compromises both safety and efficiency. In this paper, we propose a unified interaction control framework for ultrasound scanning robots capable of handling all common interactions, distinguishing both *human-intended* and *unintended* types, and adapting with appropriate compliance. Specifically, the robot suspends or modulates its ongoing main task if the interaction is *intended*, e.g., when the doctor grasps the robot to lead the end effector actively. Furthermore, it can identify *unintended* interactions and avoid potential collision in the null space beforehand. Even if that collision has happened, it can become compliant with the collision in the null space and try to reduce its impact on the main task (where the scan is ongoing) kinematically and dynamically. The multiple situations are integrated into a unified controller with a smooth transition to deal with the interactions by exhibiting human-intention-aware compliance. Experimental results validate the framework's ability to cope with all common interactions including intended intervention and unintended collision in a collaborative carotid artery ultrasound scanning task.**

I. Introduction

Ultrasound scanning is a common noninvasive health screening method in great demand. During an ultrasound scanning task, a doctor holds a scanning probe and moves it along a patient's body, maintaining close and stable contact to enable clear ultrasound imaging. Ultrasound scanning is labor-intensive, as doctors are typically required to perform several hours of imaging per day [1]. Therefore, deploying a robot to carry out these scanning tasks autonomously helps alleviate this problem [2]–[5]. To achieve this, various ultrasound scanning robots have been developed [6]–[8], and many works have been devoted to the navigation systems [9], [10], which output desired probe trajectory to obtain the ideal ultrasound image with the current ultrasound image and robot information as input. However, most works only consider the navigation while ignoring the physical interaction between the scanning robot and the human, which is an essential problem for safe ultrasound scanning.

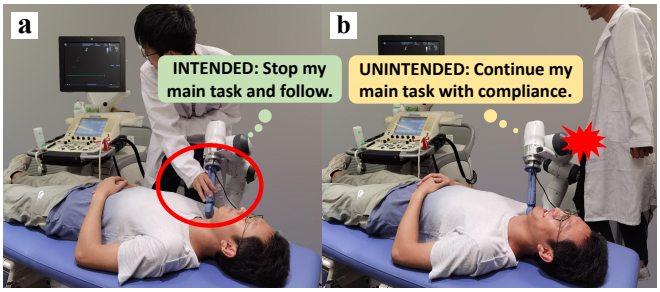

Fig. 1. An illustration of the human-intention-aware compliance during a carotid artery examination by an ultrasound scanning robot. (a) The doctor grasped the probe to apply coupling gel on the probe, and the robot stopped its current task and followed. (b) The doctor collided with the robot by his leg by accident, and the robot continued its main task with compliance.

In addition to the normal contact between the scanning probe and the patient's skin, there are many types of physical human-robot interactions commonly happening during the robot-assisted scanning, such as patients moving, doctors intervening, and doctors colliding. These interactions can be categorized into two types. i) *Human-Intended Interaction*: e.g., the doctor holds the robot end effector and actively adjust its motion (Fig. 1a); ii) *Human-Unintended Interaction*: e.g., the doctor may carelessly collide with the robot body, resulting in unexpected impacts (Fig. 1b). Different robot reactions are required for different human-robot interactions during the ultrasound scanning process.

Some existing works have applied typical interaction control methods to robotic ultrasound scanning, such as using optimization-based control [11], hybrid force/position control [12], or impedance/admittance control [8], [13], [14]. However, most works only consider the interaction between the robot and patient, neglecting the intervention from the doctor. Moreover, they usually separately dealt with single interaction situation, without achieving a unified solution for all potential interactions. Hard switching [15] between different controllers for different interaction situations will affect the smoothness and safety of the scanning process.

To address the problems, this paper proposes a unified interaction control framework for safe robotic ultrasound scanning with human-intention-aware compliance, where the robot's working mode varies according to the changing human intention. It adapts to the human-intended interactions and rejects the human-unintended ones. Specifically, this

X. Yan, Y. Jiang, M. Yu, C. Chen, G. Huang, S. Song and X. Li are with Department of Automation, Beijing National Research Center for Information Science and Technology, Tsinghua University. S. Luo is with Beijing Academy of Artificial Intelligence. S. Zhu is with Midea Corporate Research Center and State Key Laboratory of High-end Heavy-load Robots, Midea Group. This work was supported in part by the Science and Technology Innovation 2030-Key Project under Grant 2021ZD0201404, in part by the National Natural Science Foundation of China under Grant U21A20517 and 52075290, in part by the Institute for Guo Qiang, Tsinghua University, in part by the State Key Laboratory of High-end Heavy-load Robots under Grant HHR2024010426, and in part by Beijing Natural Science Foundation under Grant QY23121. Corresponding author: Xiang Li (xiangli@tsinghua.edu.cn)

framework unified achieves the following functions:

- The robot will comply with the human-intended interactions. That is, when the doctor or patient grasps the probe and actively moves it, the robot will compliantly follow the human's guidance.
- The robot will try to actively avoid human-unintended collisions between the human and robot body without affecting the main scanning task executed by the end-effector, which improves safety.
- The robot will become compliant to the external human-unintended impact when the collision or impact is unavoidable and actually happens. The achieved compliance will reduce the unsafe impact on the human without affecting the main scanning task.

The above functions are modularized as different working modes, which are integrated into a unified control framework with smooth transitions. Such a formulation is able to deal with all common physical interactions during the human-robot collaborative ultrasound scanning in a unified and smooth manner, making the human's knowledge and the robot's ability complement each other efficiently and safely. The performance of the proposed framework is validated in real-world carotid artery examinations. The key contribution of this work is summarized as follows:

- We proposed a unified control framework considering all common human-robot interactions in the human-robot collaborative ultrasound scanning task.
- We formulated different types of interactions into several modes and proposed a smooth human-intention-aware mode transition approach with weighting factors.
- We developed an integrated robotic system that achieved reliable human-robot collaborative ultrasound scanning for human carotid arteries in the real world.

II. Related works

A. Ultrasound Scanning Robots

As mentioned in the Introduction, lots of works for ultrasound scanning robots focused on navigation rather than physical interaction with humans, including intended and unintended ones, which is important for safety in a crowded clinical environment and efficiency when the human wants to intervene. The ethical and legal regulations for clinical translation and further commercialization of ultrasound scanning robots underline the importance of such interactions, that is, there must be at least one human supervisor for autonomous ultrasound scanning systems (see IEC/TR 60601-4-1 [16] formulated by *the International Organization for Standardization (ISO)* and *the International Electrotechnical Commission (IEC)*). This paper aims to further reinforce the doctor's role of supervisor, by allowing him or her to safely intervene anytime during the scanning task, with the development of a new interaction control scheme.

Moreover, most controllers for ultrasound scanning robots are designed for specific situations. A shared control method was proposed in [17] to allow both the doctor and the robot to contribute to the probe movement. That is, the doctor first moves the probe to a rough position, and the robot, regulated by an image-based visual servoing method, works to track an existing feature in ultrasonic image autonomously [2]–[4], [18]. In [15], authors proposed a hybrid force/position regulation controller for contacting and switched to a position controller for out-of-plane rotation in an aortic diameter measurement task. These works didn't consider one control framework for all common interaction situations. In this paper, a unified control framework and smooth transition for different working modes are achieved.

B. Interaction Control

Impedance control is a critical interaction control method, particularly in redundant robots. Hierarchical impedance control, including Operational Space Formulation [19]–[21] and hierarchical compliance control [22], [23], is widely used to manage robot-environment interactions. Null-space impedance control schemes, such as those in [24], enable multiple prioritized tasks at the acceleration level. Extended task space concepts [25], [26] address null-space interactions without requiring joint-torque measurements, aided by generalized force observers. In [27], a controller was proposed to ensure passivity in trajectory-tracking tasks. In [28], contact-loss stabilization was guaranteed by combining force tracking and impedance control. These approaches primarily focused on flat or regular surfaces. In contrast, [8] was able to deal with complex arbitrary surfaces in task space. Moreover, energy-tank-augmented methods [29] fixed the deterioration of passivity caused by variable impedance operation and null-space projection operation [30], [31]. The theoretical guarantee of stability and passivity helps to build a safe unified control framework in this paper.

III. Preliminaries

A. Task Definitions and Robot Dynamics

The main and secondary task coordinates and their velocities of a redundant robot can be expressed as

$$\boldsymbol{x}_1 = \boldsymbol{f}_1(\boldsymbol{q}), \quad \boldsymbol{x}_2 = \boldsymbol{f}_2(\boldsymbol{q}), \tag{1}$$

$$\dot{\boldsymbol{x}}_1 = \boldsymbol{J}_1(\boldsymbol{q})\dot{\boldsymbol{q}}, \quad \dot{\boldsymbol{x}}_2 = \boldsymbol{J}_2(\boldsymbol{q})\dot{\boldsymbol{q}}, \tag{2}$$

where $\boldsymbol{q} \in \Re^n$ is the vector of joint angles, n is the number of DOFs for a redundant robot, $\boldsymbol{x}_i \in \Re^{m_i}, i = 1, 2$ means the main and secondary task, respectively, $\boldsymbol{f}_i : \Re^n \to \Re^{m_i}$ are differentiable forward kinematic functions, $\boldsymbol{J}_i(\boldsymbol{q}) \in \Re^{m_i \times n}$ are the Jacobian matrices. The overall task dimension $m = \Sigma_{i=1}^{2} m_i = n$. The augmented task-space velocity $\dot{\boldsymbol{x}} \in \Re^n$ is

$$\dot{\boldsymbol{x}} := \begin{bmatrix} \dot{\boldsymbol{x}}_1 \\ \dot{\boldsymbol{x}}_2 \end{bmatrix} = \boldsymbol{J}(\boldsymbol{q})\dot{\boldsymbol{q}}, \tag{3}$$

where the augmented Jacobian matrix is

$$\boldsymbol{J}(\boldsymbol{q}) := \begin{bmatrix} \boldsymbol{J}_1(\boldsymbol{q}) \\ \boldsymbol{J}_2(\boldsymbol{q}) \end{bmatrix} \in \Re^{n \times n}. \tag{4}$$

A common and practical assumption [22], [23] is made to simplify the analysis:

Assumption 1: The main task and secondary task are independent and do not have singularities, i.e., $rank(\boldsymbol{J}_1) + rank(\boldsymbol{J}_2) = m_1 + m_2 = n$.

The ultrasonic scanning robot involves rich contact with doctors and patients, its dynamic model is given as

$$\boldsymbol{M}(\boldsymbol{q})\ddot{\boldsymbol{q}} + \boldsymbol{C}(\dot{\boldsymbol{q}}, \boldsymbol{q})\dot{\boldsymbol{q}} + \boldsymbol{g}(\boldsymbol{q}) = \boldsymbol{\tau} + \boldsymbol{\tau}_e, \tag{5}$$

where $\boldsymbol{M}(\boldsymbol{q}) \in \Re^{n\times n}, \boldsymbol{C}(\dot{\boldsymbol{q}}, \boldsymbol{q})\dot{\boldsymbol{q}} \in \Re^n, \boldsymbol{g}(\boldsymbol{q}) \in \Re^n$ denote the mass matrix, Coriolis and centrifugal term, and gravity vector respectively, and $\boldsymbol{\tau}, \boldsymbol{\tau}_e \in \Re^n$ represent the control torque and the external torque respectively. Note that both the contact between the scanning probe and the patient's body and the collision with the robot contributes to the external torque.

B. Hierarchically Decoupled Task and Dynamics

Since the original task coordinates are coupled between different levels, this causes difficulties in hierarchical control and stability analysis. Hierarchically decoupled task-space velocities $\boldsymbol{v}_i \in \Re^{m_i}, i \in \{1, 2\}$ are defined as[1]

$$\boldsymbol{v}_i := \bar{\boldsymbol{J}}_i \dot{\boldsymbol{q}}, \tag{6}$$

where $\bar{\boldsymbol{J}}_i$ is the decoupled Jacobian:

$$\bar{\boldsymbol{J}}_1 = \boldsymbol{J}_1, \tag{7}$$

$$\bar{\boldsymbol{J}}_1^{M+} = \boldsymbol{M}^{-1}\bar{\boldsymbol{J}}_1^T(\bar{\boldsymbol{J}}_1\boldsymbol{M}^{-1}\bar{\boldsymbol{J}}_1^T)^{-1}, \tag{8}$$

$$\bar{\boldsymbol{J}}_2 = (\boldsymbol{Z}_2\boldsymbol{M}\boldsymbol{Z}_2^T)^{-1}\boldsymbol{Z}_2\boldsymbol{M}, \tag{9}$$

where (8) is the well-known dynamically consistent inverse [19], [32]. In (9), we need to know the full row-rank null-space base matrix $\boldsymbol{Z}_2 \in \Re^{m_2\times n}$, where $\boldsymbol{Z}_2$ spans the null space of $\boldsymbol{J}_1$, i.e., $\boldsymbol{J}_1\boldsymbol{Z}_2^T = \boldsymbol{0}$. Such a matrix $\boldsymbol{Z}_2$ can be obtained by many ways like singular value decomposition or recursive methods. Here we use singular value decomposition: $\boldsymbol{J}_1 = \boldsymbol{U}\boldsymbol{\Sigma}\boldsymbol{V}^T, \boldsymbol{V} = [\boldsymbol{X}_1^T, \boldsymbol{Y}_1^T]$. We can define $\boldsymbol{Z}_1 = \bar{\boldsymbol{J}}_1^{M+T} = \boldsymbol{J}_1^{M+T}, \boldsymbol{Z}_2 = \boldsymbol{Y}_1$. Such a definition of $\boldsymbol{Z}_i$ also fulfills

$$\boldsymbol{Z}_1\bar{\boldsymbol{J}}_1^T = \boldsymbol{I}, \quad \boldsymbol{Z}_2\bar{\boldsymbol{J}}_2^T = \boldsymbol{I} \tag{10}$$

$$\boldsymbol{Z}_1\boldsymbol{M}\boldsymbol{Z}_2^T = \boldsymbol{0}. \tag{11}$$

Now, the augmented task velocity in decoupled coordinates can be defined as

$$\boldsymbol{v} := \begin{bmatrix} \boldsymbol{v}_1 \\ \boldsymbol{v}_2 \end{bmatrix} = \bar{\boldsymbol{J}}\dot{\boldsymbol{q}}, \bar{\boldsymbol{J}} := \begin{bmatrix} \bar{\boldsymbol{J}}_1 \\ \bar{\boldsymbol{J}}_2 \end{bmatrix} \tag{12}$$

According to assumption 1, $\bar{\boldsymbol{J}}$ is also non-singular. Using the properties (10)(11), a useful property can be obtained that $\bar{\boldsymbol{J}}^{-1} = [\boldsymbol{Z}_1^T, \boldsymbol{Z}_2^T]$. The variables in equation (12) will be later used for controller construction in Sec. IV-A.

IV. Methodology

We propose a unified interaction control method for ultrasound scanning robots to handle complex and dynamic interactions during scanning tasks. If the interaction is human-intended, adjust the main task to accommodate the interaction; if the interaction is unintended, only the null-space task is adapted to it without affecting the main task, as shown in Fig. 2.

[1]The dependencies are omitted in the rest of the paper for simplicity.

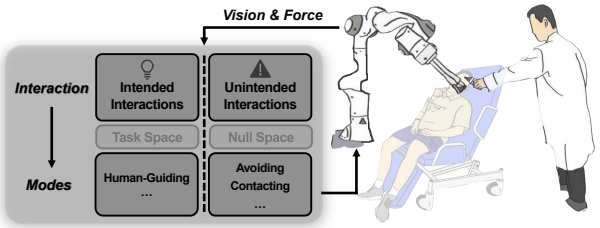

Fig. 2. The human-robot interactions considered in this work. The interactions are divided into intended- and unintended- situations and are further classified as several modes based on vision and force information.

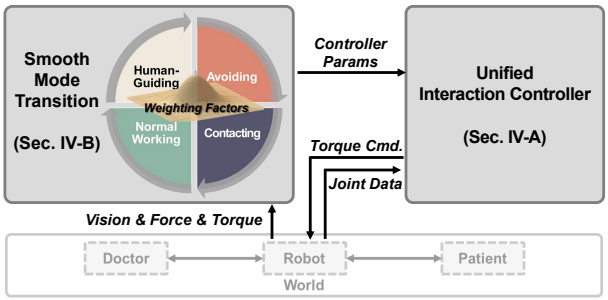

Fig. 3. The structure of our proposed method, where multiple modes are integrated into a unified control input with smooth transitions to deal with the interactions by exhibiting human-intention-aware compliance.

For this purpose, we first conclude several most common types of interaction situations during a scanning task, which are shown in the left part of Fig. 3 and more detailed in Tab. I. Three specific working modes are designed for handling interactions:

- *Human-Guiding Mode*: The robot follows the human's movement when the probe is grasped.
- *null-space Avoiding Mode*[2]: The robot adjusts its redundant joints to avoid the human when they are too close, without affecting the scan.
- *null-space Contacting Mode*: when the doctor unintentionally contacts the robot body, the robot is compliant with the contact without affecting the scanning task.

The other three modes are for normal working, which is the obligated for an ultrasound robot:

- *Scanning Mode*: The robot follows the scanning trajectory when the probe is in contact.
- *Waiting Mode*: The robot remains stationary when the trajectory is unknown.
- *Recovery Mode*: The robot re-establishes contact when the probe loses connection with the patient.

Smooth transitions between modes are critical. Existing methods rely on hard switching [11], [33], jeopardizing the stability and, hence, the safety of the human. In contrast, our method takes three steps to achieve that. First, we modified the hierarchical compliance control, with changing parameters to achieve different modes. Second, we bridge the changing parameters with perception data using smooth weighting factors. Third, we are able to show that this framework remains passive.

[2]the term "*null-space*" will be neglected in the following for simplicity.

TABLE I

POTENTIAL PHYSICAL INTERACTIONS DURING THE SCANNING AND THE DESIGNED CORRESPONDING ROBOT WORKING MODE.

FUNCTION		MODE	ROBOT BEHAVIOR	ACTIVATED WHEN
Handling Interactions	Intended	*Human-Guiding Mode*	Follow the human's movement.	Someone grasps the probe.
	Unintended	*Avoiding Mode*	Avoiding without affecting scanning task.	The doctor is too close to the robot body.
		Contacting Mode	Compliant with the contact without affecting the scanning task.	The doctor unintentionally contacts the robot body.
Normal Working		*Recovery Mode*	Recontact the patient's body.	The patient loses contact with the probe.
		Scanning Mode	Keep moving along the scanning trajectory.	The probe contacts with the patient's neck, and the scanning trajectory is given.
		Waiting Mode	Keep static.	The scanning trajectory is unknown.

A. Unified Interaction Controller Based on Hierarchical Compliance Control

We consider a redundant robot configuration which provides more flexibility for crowded hospital environment. In this paper, we use a 7-DOF manipulator and consider a 2-level hierarchy: The first level task is the end effector pose, $m_1 = 6$, which is vital in the scanning task. The secondary task is the angle of joint 1, $m_2 = 1$. Not only does such a choice meet assumption 1, but also the scalar format of the task 2 coordinate[3] makes it easier to manipulate the null-space configuration compared to other common formats like 7 DOF joint impedance.

Here, we summarize the hierarchical compliance control method [22], [23], which ensures asymptotic stability and desired impedance behavior.

The controller can be expressed as

$$\boldsymbol{\tau} = \boldsymbol{g} + \boldsymbol{\tau}_d + \boldsymbol{\tau}_1 + \boldsymbol{\tau}_2, \tag{13}$$

where $\boldsymbol{\tau}_d$ is the compensation term:

$$\boldsymbol{\tau}_d = \bar{\boldsymbol{J}}_1^T \boldsymbol{\mu}_{12} \boldsymbol{v}_2 + \bar{\boldsymbol{J}}_2^T \boldsymbol{\mu}_{21} \boldsymbol{v}_1. \tag{14}$$

One can obtain a property $\boldsymbol{\tau}_d^T \dot{\boldsymbol{q}} = \boldsymbol{0}$, indicating zero transmitted power with respect to the effort-flow pair $(\boldsymbol{\tau}_d, \dot{\boldsymbol{q}})$ [22]. The last two terms are the control torque for each subtask, which can be written as

$$\boldsymbol{\tau} = \boldsymbol{g} + \boldsymbol{\tau}_d + \boldsymbol{\tau}_1 + \boldsymbol{\tau}_2 \tag{15}$$

$$\boldsymbol{\tau}_1 = \bar{\boldsymbol{J}}_1^T \left(-\boldsymbol{K}_1 \tilde{\boldsymbol{x}}_1 - \boldsymbol{D}_1 \dot{\boldsymbol{x}}_1 \right), \tag{16}$$

$$\boldsymbol{\tau}_2 = \bar{\boldsymbol{J}}_2^T \boldsymbol{Z}_2 \boldsymbol{J}_2^T \left(-\boldsymbol{K}_2 \tilde{\boldsymbol{x}}_2 - \boldsymbol{D}_2 \dot{\boldsymbol{x}}_2 \right), \tag{17}$$

where $\tilde{\boldsymbol{x}}_i = \boldsymbol{x}_i - \boldsymbol{x}_{id}$ is the error of the ith task, $\boldsymbol{x}_{id}$ denotes the desired value of the ith task. The stiffness and damping components are represented by matrices $\boldsymbol{K}_i$ and $\boldsymbol{D}_i$, respectively. Note that these impedance parameters are time-varying during the scanning task, and hence able to be in different modes.

In *Recovery Mode*, when the probe is far away from the patient's neck, the min-jerk trajectory generator is utilized to give the desired trajectory from the current pose to the desired pose. Unlike other modes, a tracking task rather than a regulation task is requested in this mode, so we need to slightly change our controller (16) into the tracking form:

$$\boldsymbol{\tau}_1 = \bar{\boldsymbol{J}}_1^T (\ddot{\boldsymbol{x}}_{1d} - \boldsymbol{K}_1 \tilde{\boldsymbol{x}}_1 - \boldsymbol{D}_1 \dot{\tilde{\boldsymbol{x}}}_1). \tag{18}$$

Next, we will use the design of the mode identification and transition to adapt the hierarchical compliance controller to the contact-rich and dynamically interactive ultrasound scanning task with the realization of compliance that is indicated by human intention.

B. Mode Determination and Smooth Transition

The connection between different working modes is managed using five weighing factors in $[0, 1]$, each representing an aspect of the task:

1) a_h: if the probe is grasped by a human **h**and.[4];
2) a_p: if the probe is near the **p**atient's neck;
3) a_f: if the contact between the probe and the patient's neck is maintained, based on **f**orce data;
4) a_n: if the doctor contacts the robot's body, causing a **n**ull-space force;
5) a_b: if the doctor contacts the robot's **b**ody, based on position data.

To ensure a smooth transition, we define a basic function:

$$b(s) = \begin{cases} 1/1 + s^6 \ , & s \geq 0, \quad \text{(19a)} \\ 1 \, , & s < 0, \quad \text{(19b)} \end{cases}$$

The basic function is a continuous transition from 1 to 0, where s is a variable. The weighting factors are constructed through this basic function and perception data. The design of all weighting factors is detailed below.

The first and the last weighting factors a_h, a_b use position information obtained from the perception system:

$$a_h = b\left(\frac{d_h}{r_h}\right), a_b = b\left(\frac{d_b}{r_b}\right), \tag{20}$$

where d_h is the distance from the probe to one's hand and d_b is the closest distance from the robot's body to the doctor's body[5], the two scalars r_h, r_b are scaling parameters.

[3]Although task 2 coordinate is a scalar in this task, we still use boldface to represent this scalar as a vector in order to show the generality of the theory.

[4]$a_h = 1$ for true, 0 for false, the same for other factors. The bold letters show the meaning of the subscripts

[5]in the real-world experiment, "the doctor's body" is specified as the doctor's hands.

The second weighting factor also uses position information, modeling the patient's neck as a cylindrical region:

$$a_p = b\left(\frac{\sqrt{d_{py}^2 + d_{pz}^2}}{r_p}\right) \cdot b\left(\frac{|d_{px} - \frac{x_{\text{top}}+x_{\text{bottom}}}{2}|}{\frac{x_{\text{top}}-x_{\text{bottom}}}{2}}\right), \quad (21)$$

where $\boldsymbol{d}_p = [d_{px}, d_{py}, d_{pz}]^T$ is the position vector of the probe in the neck frame, r_p is the radius of the region, and $x_{\text{top}}, x_{\text{bottom}}$ are the x coordinates of the top and bottom surfaces of the region, respectively.

The third weighting factor is:

$$a_f = 1 - b\left(\frac{^E f_z}{f_0}\right), \quad (22)$$

where f_0 is a threshold constant, and $^E f_z$ denotes the force along the z-axis in the end effector frame $\{E\}$. Maintaining steady contact during scanning requires $^E f_z \geq 0$.

The fourth weighting factor a_n is defined as:

$$a_n = 1 - b\left(\frac{|\boldsymbol{\tau}_n|}{\tau_0}\right), \quad \boldsymbol{\tau}_n = \boldsymbol{\tau}_e - \boldsymbol{J}_1^T \boldsymbol{F}_{1e}, \quad (23)$$

where τ_0 is a null-space torque threshold. $\boldsymbol{\tau}_n$ is the null-space torque where $\boldsymbol{F}_{1e} \in \Re^{6\times 1}$ is the external wrench detected by the wrist-mounted F/T sensor.

The stiffness and desired task coordinates vary according to these five scalars to achieve the behaviors, as shown in Tab. I, The unified stiffness is designed as:

$$\boldsymbol{K}_{1d}(t) = (1-a_h)(1-a_f)(1-a_p)\boldsymbol{K}_{1g}, \quad (24)$$

$$\boldsymbol{K}_{2d}(t) = (1-a_h)(1-a_n)\boldsymbol{K}_{2g}, \quad (25)$$

where $\boldsymbol{K}_{1g}, \boldsymbol{K}_{2g}$ are maximum stiffness, the damping is set to be critical, i.e., the relationship between the jth diagonal entry of $\boldsymbol{D}_i$ and $\boldsymbol{K}_i$ is $d_{ij} = 2\sqrt{k_{ij}}$ for $i = \{1, 2\}$.

The desired positions $\boldsymbol{x}_{1d}, \boldsymbol{x}_{2d}$ are designed as follows. For *Waiting Mode*, $\boldsymbol{x}_{1d}, \boldsymbol{x}_{2d}$ is fixed to the pose at the moment entering this mode. Note that now the stiffness is high(all factors equal to 0), so the robot keeps still. For *Scanning Mode*, $\boldsymbol{x}_{1d}, \boldsymbol{x}_{2d}$ are given by a scanning trajectory generator in our previous work [34]. For *Recovery Mode*, $\boldsymbol{x}_{1d}, \dot{\boldsymbol{x}}_{1d}, \ddot{\boldsymbol{x}}_{1d}$ are given by a mini-jerk trajectory generator, use controller (18)(17), $\boldsymbol{x}_{2d}$ is updated to actual robot value every 100 control cycles. For *Human-Guiding Mode*, $\boldsymbol{x}_{1d}, \boldsymbol{x}_{2d}$ are set as current pose, i.e., $\boldsymbol{x}_{1d}(t) = \boldsymbol{x}_1(t), \boldsymbol{x}_{2d}(t) = \boldsymbol{x}_2(t)$). Note that in this mode, $a_h \approx 1$, the robot is soft and just follows the human. For *Avoiding Mode*, $\boldsymbol{x}_{1d}$ is the same with *Scanning Mode*, $\boldsymbol{x}_{2d} += a_b\Delta$, $\Delta \in \Re$ is a fixed step length in the secondary task, if the doctor is on right $\Delta > 0$, left $\Delta < 0$. When the doctor is no longer close to the robot body, $\boldsymbol{x}_{2d}$ will incrementally move back to its value when entering this mode. For *Contacting Mode*, $\boldsymbol{x}_{1d}, \boldsymbol{x}_{2d}$ are the same with *Scanning Mode*. Note that now $a_n = 1$, so the null-space stiffness is low, the robot will comply with the contact softly, without affecting the end effector scanning task.

The above explains how we achieve the "Robot Behavior" column in Tab. I within one framework. Another part is how to decide the "Activated When" column. We show our decision method in Alg. 1, where the subscript "t" denotes a user-defined threshold(e.g., $a_h \geq a_{ht}$ means the factor is larger than its threshold). Variable $t_p \in [0, T]$ denotes the task progress, where T is the user-defined task time. At progress time t_p, the desired pose $\boldsymbol{x}_d(t_p) = \boldsymbol{x}_d(i)$. The right term denotes the ith trajectory point, where

$$i = \left\lceil \frac{t_p \times N}{T} \right\rceil. \quad (26)$$

This human-intention detection step can also be achieved in many ways like learning-based methods.

Algorithm 1 Unified Interaction Control Algorithm

progress time $t_p = 0$
while $t_p < T$ **do**
  if $a_h \geq a_{ht}$ **then**
    Human-Guiding Mode; break;
  else if no trajectory **then**
    Waiting Mode; break;
  else if have a trajectory $\{\boldsymbol{x}_d(i)\}_{i=1}^N$ **then**
    calculate the desired pose $\boldsymbol{x}_d(t_p)$ by (26);
    if $(\|\tilde{\boldsymbol{x}}\| < \epsilon)\&\&(a_p > a_{pt})||(a_f > a_{ft})$ **then**
      if $a_b > a_{bt}$ and $a_n > a_{nt}$ **then**
        Contacting Mode; break;
      else if $a_b > a_{bt}$ and $a_n < a_{nt}$ **then**
        Avoiding Mode; break;
      else
        Scanning Mode; break;
        $t_p = t_p + dt$;
      end if
    else
      Recovery Mode; break;
    end if
  end if
end while

C. Passivity analysis

In [31], the authors augmented the hierarchical impedance controller with the energy tank method and rigorously proved the passivity property with variable impedance parameters and null-space projection. In this paper, we designed a specific time-varying way of the impedance parameters, allowing passivity to be proven similarly. This key property enables our control framework to smoothly unify different working modes while maintaining a theoretical safety guarantee. In this way, our work is distinct from other works.

V. Experiment

Real-world experiments were carried out to validate the proposed control method. The experimental setup is shown in Fig. 4. The overall system consisted of six parts: (i) an ultrasound system (Vivid E7), including an imaging machine and a probe; (ii) a 7-DOF robot manipulator (Franka Panda); (iii) an ATI mini40 FT sensor mounted between the panda arm flange and the probe; (iv) an RGBD camera (Azure Kinect DK); (v) a hospital bed (which can be folded as a

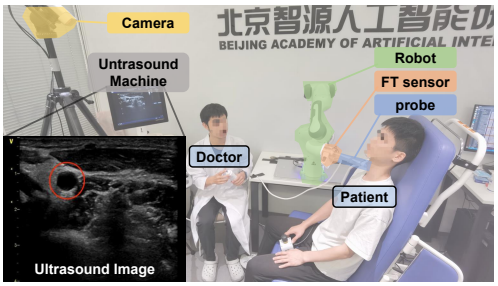

Fig. 4. The experimental setup: (a) The hardware system consists of an ultrasound machine, an RGBD camera, a manipulator, an FT sensor, an ultrasound probe, and PCs; (b) An ultrasound image, where the red circle indicates the position of the cross-section carotid artery

chair); and (vi) two PCs for processing the camera data and controlling the robot, respectively.

Using the RGBD camera, we employed the official body tracking algorithm to capture the patient's real-time neck frame and used point cloud data to generate a scanning trajectory through segmentation and reconstruction techniques. In the experiments, a human subject, simulating a patient, was seated on a hospital bed while a robot maneuvered a scanning probe along his neck to perform ultrasound imaging. A doctor was seated nearby, ready to intervene if needed.

Experiment 1 demonstrated the system's handling of intended interactions and its ability to transition between multiple interaction modes. Experiment 2 evaluated compliance with unintended interactions.

A. Experiment 1 - Transition between Multiple Modes for Intended Interactions

To simulate the complexity of the scanning task, we considered a restless patient who disrupts the process by dodging the probe, moving, sneezing, and deliberately pushing the probe. The doctor intervenes to manage unexpected situations. Stiffness varied, while damping was consistently set to be critical. Snapshots from different stages of the procedure are shown in Fig. 5[6], and the weighting factors, stiffness, error and contact force are shown in Fig. 6. The scanning task progressed as follows:

1) The *Recovery Mode* activated between 10s and 15s, gradually increasing a_p to 1, causing the scanning probe to approach the patient and establish physical contact (see Fig. 5a).
2) Between 35s and 45s, the patient pushed the probe forward twice, resulting in two peaks in ${}^{E}f_z$ and a_f. The increased tracking error $\tilde{\boldsymbol{x}}_1$ triggered *Recovery Mode*, followed by *Scanning Mode* (see Fig. 5b). During this period, a_f was crucial in attenuating k_{d1} ($\boldsymbol{K}_{1(0:3,0:3)} = k_{d1}\boldsymbol{I}$), thus limiting the contact force ${}^{E}f_z$ and ensuring patient safety and comfort.
3) During 51 s to 59 s, the probe was manually moved away from the patient's neck (see Fig. 5c), causing k_{d1} to drop to 0 along with a_h, signaling the transition to *Human-Guiding Mode* where the robot became passive and responsive to manual guidance. A similar event occurred between 79s and 95s when the doctor applied coupling gel (see Fig. 5e). Once the probe was released, k_{d1} returned to its original value. These

[6]Video at `https://yanseim.github.io/iros24ultrasound`

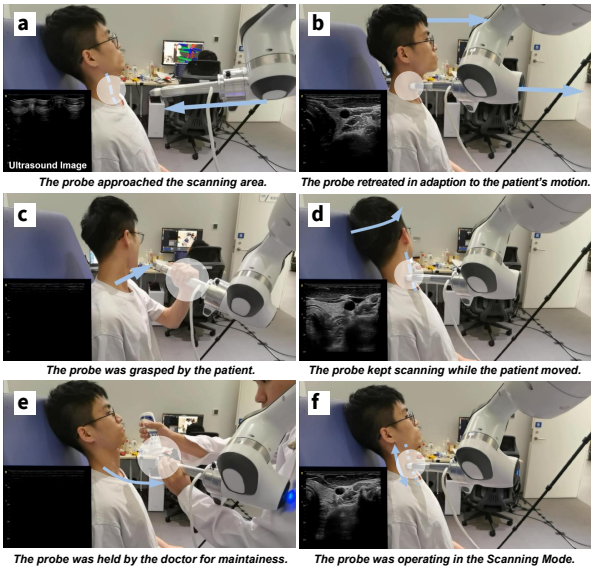

Fig. 5. Snapshots of experiment 1: (a) $t = 11.5$s. The probe was approaching the desired scanning area in the *Recovery Mode*; (b) $t = 37$s. The probe retreated while the patient tilted forward; (c) $t = 55$s. The probe was temporarily removed from the patient's neck; (d) $t = 68$s. The probe followed the desired scanning trajectory while the patient turned to the side; (e) $t = 87$s. The probe was held by the doctor for coupling gel to be applied; (f) $t = 130$s. The probe was operating in the *Scanning Mode*.

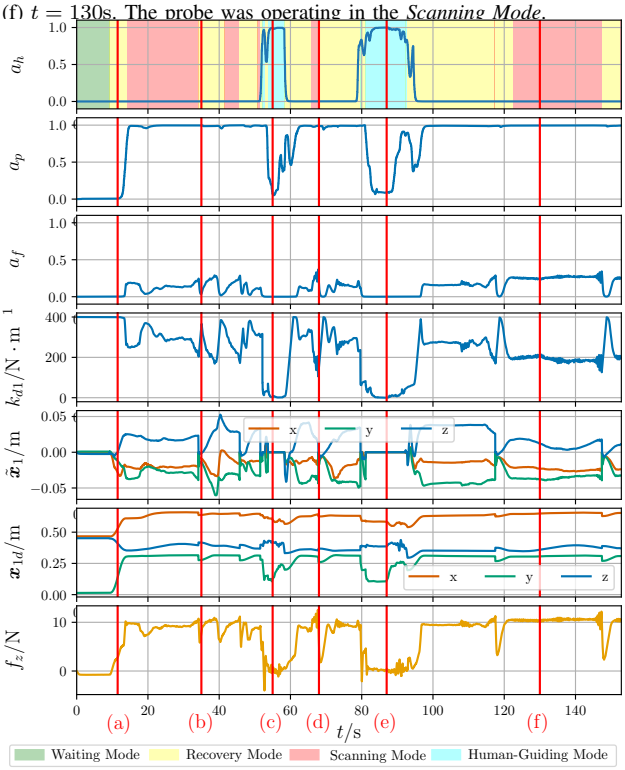

Fig. 6. Experiment 1 results, from top to bottom: the first three subfigures correspond to the weighting factors of a_h, a_p, a_f respectively; the fourth subfigure plots the translational stiffness of k_{d1}; the fifth subfigure plots the translational part of error $\tilde{\boldsymbol{x}}_1$; the sixth subfigure plots the desired translation of $\boldsymbol{x}_{1d}$; the seventh subfigure plots the estimated external force of ${}^{E}f_z$ expressed in end effector frame $\{E\}$. Background color in the first subfigure denotes different interaction modes, specifically, green - *Waiting Mode*, yellow - *Recovery Mode*, red - *Scanning Mode*, blue - *Human-Guiding Mode*. The red vertical lines denote instances in Fig. 5.

procedures showed a satisfactory reaction to intended interactions.

4) At 66s, the patient turned his head to dodge the probe (see Fig. 5d). The robot adapted and re-established contact at around 68s, reactivating *Scanning Mode*.
5) The robot operated in *Scanning Mode* between 14s and 34s and again from 122s to 146s, maintaining stable contact with $a_p \approx 1$. The contact force was adequate for high-quality imaging and safety (${}^E f_z \approx 10$ N, $a_f \leq 0.3$), with small tracking error ($\|\tilde{\boldsymbol{x}}_1\| \leq 0.04$ m).

Overall, the transitions were smooth and safety was ensured despite disturbances like patient movement or head turns. During the normal working period, the ultrasound images were clear, showing the vascular walls well. (see ultrasound images in Fig. 5).

B. Experiment 2 - Compliance to Unintended Interactions

The snapshots of experiment 2 are shown in Fig. 7. During the 32s scanning period, the doctor placed the coupling gel at around $t = 5.2$s, unintentionally activating *Avoiding Mode* (see the period in red in Fig. 8). As expected, there was no significant disturbance to the main task during *Avoiding Mode*, as seen in the $\tilde{\boldsymbol{x}}_1$ and f_z figures. The null-space configuration then recovered as designed. Then, the doctor twisted the robot's body (Fig. 7e) to simulate an unintended collision at around $t = 18.5$s. The stiffness of the secondary task dropped as in equation (25) to be compliant with the collision and hence lower the collision force as much as possible. According to the patient, the force variation on the main task (See f_z in Fig. 8) was acceptable (See video). Note that the main task error and force were not affected by the null-space modulation no matter in *Avoiding Mode* or *Contacting Mode*, showing the effectiveness of the strict hierarchy and most importantly, guaranteeing the safety and comfort of the patient and the doctor.

We conducted a user study on 9 male volunteers[6]. The results showed satisfactory robustness of our developed system on different patients.

VI. Conclusion

The proposed unified interaction control framework allows the human to safely intervene at any time during the scanning to guide the robot's movement intentionally. It also allows the robot to avoid or partially accept unexpected collisions with humans by exhibiting compliance in null space without affecting the ongoing scanning task, ensuring patient safety. The system can distinguish between intended and unintended interactions, adapting the main task to the former and the null-space task to the latter. Experimental results from a carotid examination demonstrate that the system's human-intention-aware compliance ensures safety, comfort, convenience, and autonomous scanning, even with significant patient movement, doctor involvement, and unforeseen changes. Our future work will be devoted to the development of more comprehensive human intention estimation approaches based on more types of human feedback.

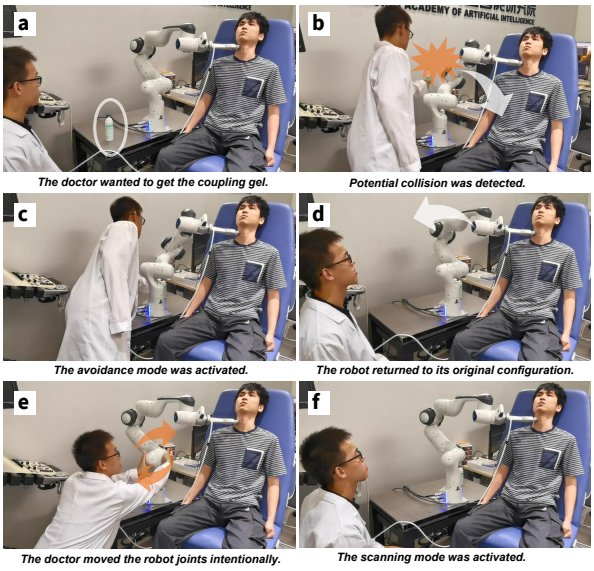

Fig. 7. Snapshots of experiment 2: (a) $t = 2.5$s. The robot was performing the scanning task. (b) $t = 5.2$s. The doctor wanted to put the coupling gel on the back of the robot. The robot detected the potential collision and entered *Avoiding Mode*. (c) $t = 7.0$s. The *Avoiding Mode* enabled the doctor to the place conveniently. (d) $t = 10.0$s. The robot returned to its original configuration for scanning. (e) $t = 19.0$s. The doctor contacted the robot in the null space, the *Contacting Mode* was activated, and the error and force of the end effector main task were unaffected. (f) $t = 25.0$s. The *Scanning Mode* was activated.

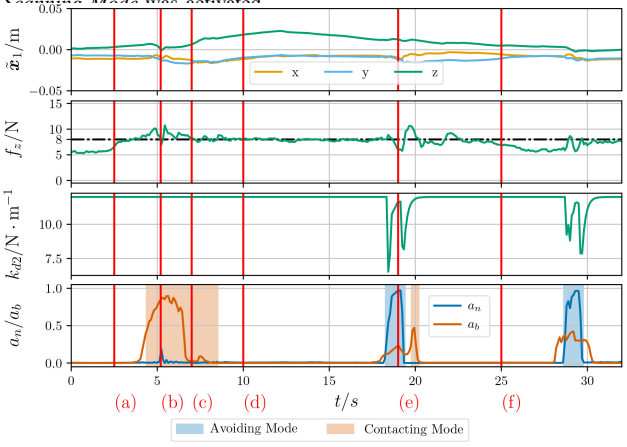

Fig. 8. Experiment 2 results, from top to bottom: the position error of the main task; the contact force in the z direction of the end effector frame ${}^E f_z$; the stiffness of the secondary task k_{d2}; weighting factors a_n, a_b. Background color in the last subfigure denotes different interaction modes, specifically, red - *Avoiding Mode*, blue - *Contacting Mode*. The red vertical lines denote instances in Fig. 7.

References

[1] hopkins medicine, "Cardiac sonography training." Website, 2022. https://www.hopkinsmedicine.org/heart_vascular_institute/education/cardiac-sonography/.

[2] C. Hennersperger, B. Fuerst, S. Virga, O. Zettinig, B. Frisch, T. Neff, and N. Navab, "Towards mri-based autonomous robotic us acquisitions: a first feasibility study," *IEEE transactions on medical imaging*, vol. 36, no. 2, pp. 538–548, 2016.

[3] R. Kojcev, B. Fuerst, O. Zettinig, J. Fotouhi, S. C. Lee, B. Frisch, R. Taylor, E. Sinibaldi, and N. Navab, "Dual-robot ultrasound-guided needle placement: closing the planning-imaging-action loop," *International journal of computer assisted radiology and surgery*, vol. 11, no. 6, pp. 1173–1181, 2016.

[4] P. Chatelain, A. Krupa, and N. Navab, "Confidence-driven control of an ultrasound probe," *IEEE Transactions on Robotics*, vol. 33, no. 6, pp. 1410–1424, 2017.

[5] H. Jiang, Z. Sun, N. Jia, M. Li, Y. Sun, S. Luo, S. Song, and G. Huang, "Cardiac copilot: Automatic probe guidance for echocardiography with world model," *arXiv preprint arXiv:2406.13165*, 2024.

[6] K. Li, Y. Xu, and M. Q.-H. Meng, "An overview of systems and techniques for autonomous robotic ultrasound acquisitions," *IEEE Transactions on Medical Robotics and Bionics*, vol. 3, no. 2, pp. 510–524, 2021.

[7] M. K. Welleweerd, A. G. de Groot, V. Groenhuis, F. J. Siepel, and S. Stramigioli, "Out-of-plane corrections for autonomous robotic breast ultrasound acquisitions," in *2021 IEEE International Conference on Robotics and Automation (ICRA)*, pp. 12515–12521, IEEE, 2021.

[8] M. Dyck, A. Sachtler, J. Klodmann, and A. Albu-Schäffer, "Impedance control on arbitrary surfaces for ultrasound scanning using discrete differential geometry," *IEEE Robotics and Automation Letters*, vol. 7, no. 3, pp. 7738–7746, 2022.

[9] K. Li, Y. Xu, J. Wang, D. Ni, L. Liu, and M. Q.-H. Meng, "Image-guided navigation of a robotic ultrasound probe for autonomous spinal sonography using a shadow-aware dual-agent framework," *IEEE Transactions on Medical Robotics and Bionics*, vol. 4, no. 1, pp. 130–144, 2021.

[10] Y. Bi, Z. Jiang, Y. Gao, T. Wendler, A. Karlas, and N. Navab, "Vesnet-rl: Simulation-based reinforcement learning for real-world us probe navigation," *IEEE Robotics and Automation Letters*, 2022.

[11] A. Duan, M. Victorova, J. Zhao, Y. Sun, Y. Zheng, and D. Navarro-Alarcon, "Ultrasound-guided assistive robots for scoliosis assessment with optimization-based control and variable impedance," *IEEE Robotics and Automation Letters*, vol. 7, no. 3, pp. 8106–8113, 2022.

[12] R. Goel, F. Abhimanyu, K. Patel, J. Galeotti, and H. Choset, "Autonomous ultrasound scanning using bayesian optimization and hybrid force control," in *2022 International Conference on Robotics and Automation (ICRA)*, pp. 8396–8402, IEEE, 2022.

[13] J. Fu, I. Burzo, E. Iovene, J. Zhao, G. Ferrigno, and E. De Momi, "Optimization-based variable impedance control of robotic manipulator for medical contact tasks," *IEEE Transactions on Instrumentation and Measurement*, 2024.

[14] R. Finocchi, F. Aalamifar, T. Y. Fang, R. H. Taylor, and E. M. Boctor, "Co-robotic ultrasound imaging: A cooperative force control approach," in *Medical Imaging 2017: Image-Guided Procedures, Robotic Interventions, and Modeling*, vol. 10135, pp. 270–280, SPIE, 2017.

[15] S. Virga, O. Zettinig, M. Esposito, K. Pfister, B. Frisch, T. Neff, N. Navab, and C. Hennersperger, "Automatic force-compliant robotic ultrasound screening of abdominal aortic aneurysms," in *2016 IEEE/RSJ International Conference on Intelligent Robots and Systems (IROS)*, pp. 508–513, 2016.

[16] ISO and IEC, "Iec/tr 60601-4-1." https://www.iso.org/obp/ui/en/#iso:std:iec:tr:60601:-4-1:ed-1:v1:en, 2017. Accessed: 2024-01-08.

[17] M. Selvaggio, M. Cognetti, S. Nikolaidis, S. Ivaldi, and B. Siciliano, "Autonomy in physical human-robot interaction: A brief survey," *IEEE Robotics and Automation Letters*, 2021.

[18] R. Nakadate, J. Solis, A. Takanishi, E. Minagawa, M. Sugawara, and K. Niki, "Implementation of an automatic scanning and detection algorithm for the carotid artery by an assisted-robotic measurement system," in *2010 IEEE/RSJ International Conference on Intelligent Robots and Systems*, pp. 313–318, IEEE, 2010.

[19] O. Khatib, "A unified approach for motion and force control of robot manipulators: The operational space formulation," *IEEE Journal on Robotics and Automation*, vol. 3, no. 1, pp. 43–53, 1987.

[20] J. Nakanishi, R. Cory, M. Mistry, J. Peters, and S. Schaal, "Operational space control: A theoretical and empirical comparison," *The International Journal of Robotics Research*, vol. 27, no. 6, pp. 737–757, 2008.

[21] A. Dietrich, C. Ott, and J. Park, "The hierarchical operational space formulation: Stability analysis for the regulation case," *IEEE Robotics and Automation Letters*, vol. 3, no. 2, pp. 1120–1127, 2018.

[22] C. Ott, A. Kugi, and Y. Nakamura, "Resolving the problem of non-integrability of nullspace velocities for compliance control of redundant manipulators by using semi-definite lyapunov functions," in *2008 IEEE international conference on robotics and automation*, pp. 1999–2004, IEEE, 2008.

[23] C. Ott, A. Dietrich, and A. Albu-Schäffer, "Prioritized multi-task compliance control of redundant manipulators," *Automatica*, vol. 53, pp. 416–423, 2015.

[24] H. Sadeghian, L. Villani, M. Keshmiri, and B. Siciliano, "Multi-priority control in redundant robotic systems," in *2011 IEEE/RSJ International Conference on Intelligent Robots and Systems*, pp. 3752–3757, IEEE, 2011.

[25] Y. Oh, W. Chung, and Y. Youm, "Extended impedance control of redundant manipulators based on weighted decomposition of joint space," *Journal of Robotic Systems*, vol. 15, no. 5, pp. 231–258, 1998.

[26] H. Sadeghian, L. Villani, M. Keshmiri, and B. Siciliano, "Task-space control of robot manipulators with null-space compliance," *IEEE Transactions on Robotics*, vol. 30, no. 2, pp. 493–506, 2013.

[27] K. Kronander and A. Billard, "Passive interaction control with dynamical systems," *IEEE Robotics and Automation Letters*, vol. 1, no. 1, pp. 106–113, 2015.

[28] C. Schindlbeck and S. Haddadin, "Unified passivity-based cartesian force/impedance control for rigid and flexible joint robots via task-energy tanks," in *2015 IEEE international conference on robotics and automation (ICRA)*, pp. 440–447, IEEE, 2015.

[29] F. Ferraguti, C. Talignani Landi, L. Sabattini, M. Bonfè, C. Fantuzzi, and C. Secchi, "A variable admittance control strategy for stable physical human–robot interaction," *The International Journal of Robotics Research*, vol. 38, no. 6, pp. 747–765, 2019.

[30] A. Dietrich, X. Wu, K. Bussmann, C. Ott, A. Albu-Schäffer, and S. Stramigioli, "Passive hierarchical impedance control via energy tanks," *IEEE Robotics and Automation Letters*, vol. 2, no. 2, pp. 522–529, 2016.

[31] Y. Michel, C. Ott, and D. Lee, "Safety-aware hierarchical passivity-based variable compliance control for redundant manipulators," *IEEE Transactions on Robotics*, vol. 38, no. 6, pp. 3899–3916, 2022.

[32] A. Dietrich, C. Ott, and A. Albu-Schäffer, "An overview of null space projections for redundant, torque-controlled robots," *The International Journal of Robotics Research*, vol. 34, no. 11, pp. 1385–1400, 2015.

[33] Q. Huang, B. Wu, J. Lan, and X. Li, "Fully automatic three-dimensional ultrasound imaging based on conventional b-scan," *IEEE transactions on biomedical circuits and systems*, vol. 12, no. 2, pp. 426–436, 2018.

[34] X. Yan, Y. Jiang, G. Wu, C. Chen, G. Huang, and X. Li, "Multi-modal interaction control of ultrasound scanning robots with safe human guidance and contact recovery," *arXiv preprint arXiv:2302.05685*, 2023.